Environmental Research 186 (2020) 109513

Contents lists available at ScienceDirect

Environmental Research

journal homepage: www.elsevier.com/locate/envres

Aquatic toxicity and mode of action of CdS and ZnS nanoparticles in four microalgae species

Konstantin Pikula[a,b,*], Neli Mintcheva[c,d], Sergei A. Kulinich[a,c,e], Alexander Zakharenko[a,b], Zhanna Markina[a,f], Vladimir Chaika[a], Tatiana Orlova[a,f], Yaroslav Mezhuev[g], Emmanouil Kokkinakis[h], Aristidis Tsatsakis[h,i], Kirill Golokhvast[a,b,j]

[a] Far Eastern Federal University, Vladivostok, 690950, Russian Federation
[b] N.I. Vavilov All-Russian Research Institute of Plant Genetic Resources, Saint Petersburg, 190121, Russian Federation
[c] Research Institute of Science and Technology, Tokai University, Hiratsuka, Kanagawa, 259-1292, Japan
[d] Department of Chemistry, University of Mining and Geology, Sofia, 1700, Bulgaria
[e] Department of Mechanical Engineering, Tokai University, Hiratsuka, Kanagawa, 259-1292, Japan
[f] A.V. Zhirmunsky National Scientific Center of Marine Biology, Far Eastern Branch, Russian Academy of Sciences, Vladivostok, 690014, Russian Federation
[g] Mendeleev University of Chemical Technology of Russia, Moscow, 125047, Russian Federation
[h] Laboratory of Toxicology, School of Medicine, University of Crete, Heraklion, 71003, Greece
[i] I.M. Sechenov First Moscow State Medical University, Moscow, 119048, Russian Federation
[j] Pacific Geographical Institute FEB RAS, Vladivostok, 690014, Russian Federation

ARTICLE INFO

Keywords:
Aquatic toxicity
CdS
Microalgae
Nanoparticles
ZnS. This work was supported by the Russian foundation for basic research (project number 19-05-50010)

ABSTRACT

This study reports the differences in toxic action between cadmium sulfide (CdS) and zinc sulfide (ZnS) nanoparticles (NPs) prepared by recently developed xanthate-mediated method. The aquatic toxicity of the synthesized NPs on four marine microalgae species was explored. Growth rate, esterase activity, membrane potential, and morphological changes of microalgae cells were evaluated using flow cytometry and optical microscopy.

CdS and ZnS NPs demonstrated similar level of general toxicity and growth-rate inhibition to all used microalgae species, except the red algae *P. purpureum*. More specifically, CdS NPs caused higher inhibition of growth rate for *C. muelleri* and *P. purpureum*, while ZnS NPs were more toxic for *A. ussuriensis* and *H. akashiwo* species. Our findings suggest that the sensitivity of different microalgae species to CdS and ZnS NPs depends on the chemical composition of NPs and their ability to interact with the components of microalgal cell-wall. The red microalga was highly resistant to ZnS NPs most likely due to the presence of phycoerythrin proteins in the outer membrane bound Zn^{2+} cations defending their cells from further toxic influence. The treatment with CdS NPs caused morphological changes and biochemical disorder in all tested microalgae species. The toxicity of CdS NPs is based on their higher photoactivity under visible light irradiation and lower dissociation in water, which allows them to generate more reactive oxygen species and create a higher risk of oxidative stress to aquatic organisms.

The results of this study contribute to our understanding of the parameters affecting the aquatic toxicity of semiconductor NPs and provide a basis for further investigations.

1. Introduction

Metal-oxide and metal-sulfide nanoparticles (NPs), including cadmium and zinc sulfides (CdS and ZnS), are often used for oxidation of organic matter during sewage water treatment owing to their photocatalytic properties (Belver et al., 2019; Mansour et al., 2020). Moreover, CdS and ZnS nanocrystals are known for their successful applications not only in pollutant removal but also for the reduction of carbon dioxide, aldehydes, water splitting, and reductive dehalogenation of benzene derivatives (Xu et al., 2019). The separation of nanosized catalysts from the reaction mixture is often limited, which allows such NPs to appear and accumulate in natural water bodies, presenting serious threats to aquatic organisms (Kumari et al., 2019; Matos et al., 2020).

Degradation of organic pollutants with semiconductor photocatalysts is based on their ability to initiate oxidation processes through

* Corresponding author. Far Eastern Federal University, Vladivostok, 690950, Russian Federation.
E-mail address: pikula_ks@dvfu.ru (K. Pikula).

https://doi.org/10.1016/j.envres.2020.109513
Received 2 April 2020; Received in revised form 9 April 2020; Accepted 9 April 2020
Available online 14 April 2020
0013-9351/

the generation of reactive oxygen species (ROS) after photoexcitation (Belver et al., 2019; Zhang et al., 2019). However, because of photochemical processes and dissociation, these types of particles can release toxic metal ions into the aquatic environment (Balmuri et al., 2017; Bedia et al., 2019; Deng et al., 2019). Corrosion and low stability of semiconductor NPs in aqueous media are considered important among the most serious concerns restricting their use for water purification. Therefore, safe and efficient photocatalyst must have high photocatalytic activity, high chemical stability, and low toxicity (Singh et al., 2020).

Aquatic organisms are often used in toxicology and ecotoxicology risk assessment studies due to their sensitivity, ubiquity, and simplicity of cultivation. Several reports have demonstrated high aquatic toxicity of cadmium and zinc-based semiconductor NPs. For example, toxic effect of cadmium selenide and zinc selenide NPs was demonstrated in tests with planktonic crustacean *Daphnia magna* (Kim et al., 2010). Similarly, toxicity of different types of CdS NPs was shown for bacterium *Vibrio fischeri*, microalgae *Raphidocelis subcapitata* and *Chlorella vulgaris*, for *Daphnia magna* (Silva et al., 2016). Importantly, the toxicity of these NPs is not limited to planktons, bacteria, and microalgae but they are also toxic for aquatic plants such as *Spirodela polyrrhiza* (Khataee et al., 2014), while ZnS NPs were tested using clam *Ruditapes decussatus* (Labiadh et al., 2017). Though a wide range of NPs have been tested for their toxicity to different life forms but the mode of toxic action of metal sulfide NPs is not fully understood yet.

This study aims to contribute to the above-mentioned area of research by exploring the aquatic toxicity of CdS and ZnS NPs prepared by a recently developed xanthate-mediated method using microalgae-bioassay approach. Microalgae can be highlighted among aquatic test organisms that are widely distributed in the ocean and represent the initial trophic level of food chains (Perez-Garcia et al., 2011). Any processes and substances affecting their population can cause consequences for higher trophic levels, which is why investigating toxicity effects on such species is very important in order to facilitate designing of safer NPs and introducing of new regulations (Piperigkou et al., 2016; Pikula et al., 2020a).

2. Materials and methods

2.1. Preparation and characterization of CdS and ZnS nanoparticles

CdS and ZnS NPs were synthesized in the University of Mining and Geology, St. Ivan Rilski (Sofia, Bulgaria) (Mintcheva et al., 2019). Potassium ethylxanthate, $C_2H_5OCS_2K$ (Acros organics, Geel, Belgium) was used as a precursor and source of sulfide ions. In basic solution at elevated temperatures, the xanthate anion is unstable and decomposes to monothiol carbonate, alcohol, and hydrogen sulfide ion. The latter is deprotonated to sulfide ion (S^{2-}) which can form metal sulfide NPs in a controllable way.

The experimental procedure for preparation of CdS NPs is described as follows: 40 ml of aqueous solution of potassium ethylxanthate (0.400 g, or 0.0025 mol) and 0.200 g of KOH (0.0036 mol, Teocom, Sofia, Bulgaria) dissolved in 5 ml of distilled H_2O were mixed in a flask and heated at 65 °C under continuous stirring for 1 h. The second solution was prepared from 0.7712 g of $Cd(NO_3)_2$ (0.0025 mol, Teocom, Sofia, Bulgaria) in 12 ml of H_2O and then added drop-by-drop to the xanthate solution. The resulting mixture was heated at 80 °C under reflux for 3 h. Then it was cooled to room temperature and the formed precipitate was separated by centrifugation and washed several times with water and ethanol. The product was dried at 230 °C for 2 h in an oven. The ZnS NPs were prepared under similar conditions. The only difference was that the $Cd(NO_3)_2$ was replaced by 0.7438 g of Zn $(NO_3)_2{\cdot}6H_2O$ (0.0025 mol, Teocom, Sofia, Bulgaria), while ZnS NPs were prepared (Mintcheva et al., 2019).

Scanning electron microscopy (SEM) and transmission electron microscopy (TEM) were used to characterize the obtained NPs, using JSM-6010PLLIS/LA and JEM 2100 tools (both from JEOL Ltd., Japan), respectively. Phase identification of NPs was performed by X-ray diffraction (XRD) analysis which was carried out with a Bruker D2 Phaser instrument (Cu/Ni radiation, $\lambda = 0.154184$ nm).

Table 1
Microalgae cultivation and experimental conditions.

Parameters	Cultivation conditions
Temperature	20 ± 2 °C
pH	8.0 ± 0.2
Salinity	33 ± 1‰
Light intensity	300 μmol $m^{-2}{\cdot}s^{-1}$, cool white fluorescent
Light cycle	12:12 h light:dark
Test type	Flow cytometry
Test chamber	24-well plate
Age of test organisms	14–20 d, exponential growth phase
Initial bioassay cell density	1–5 × 10^3 cells ml^{-1}
Control/diluent water	f/2 medium/0.22 μm filtered seawater
Test endpoints	**Test conditions** (dye or marker/test duration/emission filter)
Growth inhibition/viability	Propidium iodide/24 h, 96 h, 7 days/610 nm (FL1)
Esterase activity	Fluorescein diacetate/3 h, 24 h/525 nm (FL2)
Membrane potential	3,3′-dihexyloxacarbocyanine iodide/6 h, 24 h/525 nm (FL2)
Size	Size calibration kit/96 h, 7 days/forward scatter of blue laser (FSC)

2.2. Microalgae bioassay

Microalgal cultures were originally isolated from the sea water samples taken from Peter the Great Bay (Sea of Japan, Far-Eastern Russia) and were provided by the Resource Collection *Marine biobank* of the National Scientific Center of Marine Biology, Far Eastern Branch of the Russian Academy of Sciences (NSCMB FEB RAS). The test-species included two marine diatoms *Attheya ussuriensis* and *Chaetoceros muelleri*, a red algae *Porphyridium purpureum* (Drew and Ross, 1965), and a Raphidophyte *Heterosigma akashiwo* (Hara and Chihara, 1987). Microalgae cells were cultured with Guillard's f/2 medium, as reported earlier (Pikula et al., 2020b).

Both culturing of microalgae and toxicity tests were conducted following the guidance of OECD No.201 (OECD, 2011) with minor modifications (Table 1). For bioassays, algal cultures growing in the exponential growth phase were used. For microalgae cultivation, 24-well plates with CdS and ZnS NPs at concentrations of 1, 10, and 100 mg/l were used. The wells with only f/2 medium were taken as a control group. All assays for each concentration of NPs were conducted in four replications. The volume of microalgae aliquots in each replication was 2 ml.

Registration of cell death and biochemical changes of microalgae cells after exposure to NPs were monitored in a flow cytometer CytoFLEX (Beckman Coulter, USA) with the software package CytExpert v.2.0. The toxic level assessment and determination of algal biochemical changes were evaluated using specific fluorescent dyes (Molecular Probes, USA). A blue laser (488 nm) of the CytoFLEX flow cytometer was chosen as a source of excitation light since this wavelength matches the absorption maximum of used dyes and their metabolites. The emission filters were selected according to the maximum emission of the dyes provided by the manufacturer (Molecular Probes, USA). The chosen filters were used to record the fluorescence of each dye and its metabolites. Each sample was measured at a flow rate of 100 μl/min for 30 s. The registration time for used endpoints were selected according to the standard methods commonly used to assess toxicity of a test substance in an aqueous system with microalgae model organisms (Gao et al., 2011; Perry et al., 2011; Prado et al., 2012).

To determine the number of microalgae cells in each measurement,

a homogeneous population of events was selected on the FSC/SSC dot cytogram (forward scattering to side scattering ratio). The next stage was to separate microalgae cells from the chosen population of events by registering the fluorescence of chlorophyll *a* in the emission filter FL3 (690 nm) of the CytoFLEX flow cytometer.

Cell viability was determined by staining with propidium iodide (PI) according to the standard bioassay protocol (Crowley et al., 2016). The mechanism of PI action is the incorporation between DNA or RNA base pairs, whereupon the dye increases its fluorescence intensity by 20–30 times (Suzuki et al., 1997). Since PI is not able to penetrate intact membranes of living cells, the cells with dramatically increased fluorescent intensity in the emission filter FL1 (610 nm), in comparison with the control sample, can be regarded as dead cells. The calculation of live microalgae cells was performed by identifying cells that have chlorophyll *an* autofluorescence and by excluding dead cells. The 96 h and 7 days half maximal effective concentration (EC_{50}) of microalgae growth-rate inhibition are one of the most common values used for evaluation of cytotoxic effects in macroalgae bioassay (Zhao et al., 2018; Nikitin et al., 2019).

Esterase activity of microalgae exposed to CdS and ZnS NPs was evaluated using non-fluorescent lipophilic dye fluorescein diacetate (FDA). Fluorescein diacetate can easily penetrate the microalgae cell wall and then decompose through interaction with nonspecific esterases inside the cell to form a brightly fluorescent constituent called fluorescein (Fontvieille et al., 1992). Thus, according to the intensity of fluorescein fluorescence inside the cells, registered in the emission filter FL2 (525 nm), the esterase activity of microalgae can be evaluated as a sensitive endpoint of algal sublethal toxicity (Wang et al., 2016). Changes of microalgae esterase activity are mostly caused by the deficiency of enzyme action or by disruption of membrane integrity, and it can be evaluated as a sensitive endpoint of algal sublethal toxicity (Wang et al., 2016). The 3 h and 24 h registration points were chosen to detect possible early metabolic response of the algae over short exposure periods and dynamic change of that response, respectfully (Prado et al., 2012).

Membrane potential of microalgae cells was assessed by a lipophilic, positively charged fluorescent dye 3,3′-dihexyloxacarbocyanine iodide ($DIOC_6$), which is capable of binding to membranes (mitochondria and endoplasmic reticulum) and other hydrophobic negatively charged cell structures (Sabnis et al., 1997). In cases where the inner membrane of the cell was more electronegative in comparison to medium (hyperpolarization, i.e. an increase in the membrane potential), the dye will be absorbed. If the membrane potential increases and the cell becomes less electronegative compared to the medium (depolarization), the dye will be removed from the cell (Grégori et al., 2003). Therefore, the membrane potential change of microalgae cells affected by CdS and ZnS NPs was registered in the emission filter FL2 (525 nm) and compared with the control group. Changes of membrane potential can be accompanied by changes of membrane elasticity, loss of lipid microdomains, and changes of ion permeability (Seong and Lee, 2017). Integrity and normal operation of membranes are vital parameters for organisms as they provide barriers and transportation functions. The 6 h and 24 h registration points were chosen to detect changes in membrane potential of microalgae cells (Perry et al., 2011).

Before the assessment of growth-inhibition, esterase activity, and membrane potential of each microalgae species, a series of preliminary measurements were made to determine the optimal concentration of fluorescent dyes and the optimal duration of staining as described in our previous work (Pikula et al., 2019a). The results of this optimization are summarized in Table 2. All the data of flow cytometric measurement analysis were interpreted as the mean fluorescence intensity.

Morphological changes of microalgae cells were captured by an optical microscope Axio Observer A1 (Carl Zeiss, Germany).

2.3. Statistical analysis

Statistical analyses were performed using the software package GraphPad Prism 7.04 (GraphPad Software, USA). The one-way ANOVA test was used for analysis. A value of $p \leq 0.05$ was considered statistically significant.

3. Results

3.1. Characteristics of CdS and ZnS nanoparticles

The composition of metal sulfide samples was confirmed by powder X-ray diffraction and energy-dispersive X-ray spectroscopy (EDX) data. The XRD patterns demonstrated the cubic crystal phase of both CdS and ZnS (Fig. 1). The peaks observed at 2θ values of 26.5, 30.5, 43.9, and 52.0 were assigned to the reflection planes (111), (200), (220), and (311) of cubic CdS (JCPDS 75–1546). The corresponding peaks of ZnS are indexed for zinc blende type (JCPDS 05–0566). Based on the XRD patterns, the average crystallite size was calculated to be 6.3 nm and 3.9 nm for CdS and ZnS, respectively. More specifically, the size was found by using the Scherrer's equation, $L = 0.9\lambda/(B\cos\theta)$, where L is the coherence length, λ is the wavelength of the X-ray radiation (0.15406 nm), B is the full-width at half-maximum intensity (FWHM) of the most intense peak, and θ is the angle of diffraction. The relationship between the coherence length (L) and the diameter of the spherical crystallite (D) is known to be $D = 4l/3$. The values of crystallites size are in good agreement with those obtained from TEM analysis of both nanomaterials and reported elsewhere, namely the average diameter of CdS and ZnS crystallites is 7.0 nm and 4.2 nm, respectively (Mintcheva et al., 2019). No peaks of impurities of other crystalline phases were observed in the XRD patterns (Fig. 1), while presence of amorphous products of ZnS hydrolysis cannot be excluded, as can be seen from EDX results indicating lower sulfur content than expected. The EDX data of CdS clearly show that the product consists of Cd and S with an atomic ratio nearly of 1:1 (48.48:51.52 at. %, respectively) (Mintcheva et al., 2019).

The surface morphology of CdS and ZnS NPs was studied by SEM and TEM methods and the corresponding images are presented in Fig. 2 and Fig. 3. The SEM images demonstrate that both materials are quite narrow in size distribution and consist of well-dispersed sphere-like particles. The TEM images confirm that the nanocrystals are approximately monodispersed and have the estimated sizes in the range 5.0–9.0 nm and 2.6–5.6 nm for CdS and ZnS, respectively (Mintcheva et al., 2019).

3.2. Results of microalgae-bioassay

We calculated the concentrations that caused 50% inhibition of viability, esterase activity, and membrane potential and the results were summarized in Table 3.

The growth rate of *A. ussuriensis*, *H. akashiwo*, and *C. muelleri* decreased significantly over time by both types of NPs. The diatom algae *C. muelleri* demonstrated the highest sensitivity to both CdS and ZnS after 96 h and seven days of exposure to their NPs (Table 3). For these microalgae species, the calculated seven-day EC_{50} concentrations of growth rate inhibition were 3.0 mg/l and 4.2 mg/l for CdS and ZnS, respectively. In contrast, the red algae *P. purpureum* demonstrated tolerance to ZnS, and the calculated EC_{50} was 197.5 mg/l.

The esterase activity of microalgae species *A. ussuriensis* and *H. akashiwo* decreased significantly after 3 h of exposure to NPs. However, the effect was partly eliminated by 24 h of exposure. The esterase activity of *P. purpureum* remained stable at the point of 3-h exposition with both studied types of NPs, but the enzyme activity of the microalgae cells was significantly inhibited for 24 h exposure to CdS. The esterase activity of *C. muelleri* maintained the same level even at high NP concentrations.

Table 2
Microalgae staining parameters.

Species	Growth inhibition/Vitality (Staining with PI)		Esterase Activity (Staining with FDA)		Membrane Potential (Staining with $DIOC_6$)	
	Concentration, μM	Staining duration, min	Concentration, μM	Staining duration, min	Concentration, μM	Staining duration, min
A. ussuriensis	7.5	5–30	5.0	28–32	0.5	20–30
H. akashiwo	15.0	10	5.0	26–34	0.5	20–30
C. muelleri	10.0	30	5.0	8–12	0.1	15–35
P. purpureum	40.0	5	15.0	18–28	1.5	15–25

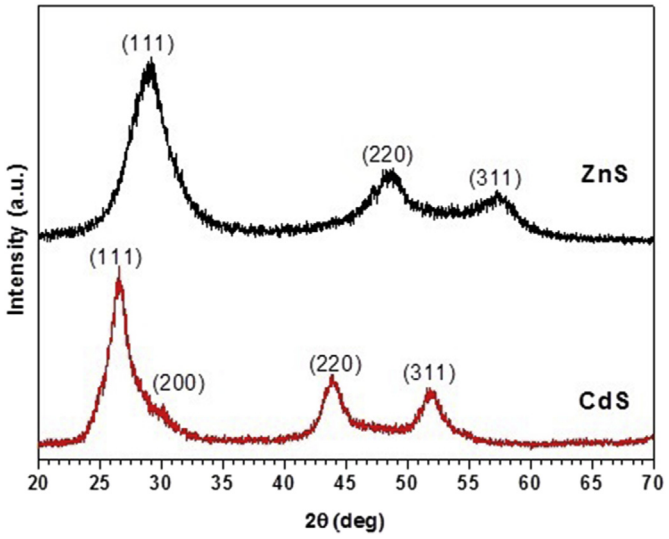

Fig. 1. XRD diffraction patterns of as-prepared CdS and ZnS nanoparticles.

Membrane depolarization was registered for all tested microalgae species affected by CdS NPs. Moreover, the depolarization effect increased with time. ZnS NPs showed a lower impact on the electric potential of microalgal cell membranes, and the influence noticeably decreased by 24 h of exposure for all algal species.

The changes of microalgae cell size upon exposure to CdS and ZnS nanomaterials, according to the data from flow cytometry analysis, are represented in Fig. 4. Significant enlargement of cell size was detected for *C. muelleri* at the concentration of 10 mg/l of CdS (Fig. 4c) and for red algae *P. purpureum* at the concentration of 100 mg/l of CdS (Fig. 4d).

Visual observation by optical microscopy has shown the most noticeable changes for the red algae *P. purpureum* (Fig. 5). Microscopy observation of *P. purpureum* confirms enlargement of cell size caused by the effect of CdS NPs (Fig. 5b), which is in accordance with the data of flow cytometry (Fig. 4). Moreover, it was found that part of the red algae cells changed their pigmentation after exposure to ZnS (Fig. 5c).

4. Discussion

4.1. Growth-rate inhibition and general toxicity

Following the aim of this research, here we compared two types of semiconductor NPs in terms of their effect on the level of aquatic toxicity. The growth-rate inhibition of microalgae can be considered as a marker of general toxicity. The results of our previous work with the same microalgae species (Pikula et al., 2019b) showed the following trend in microalgae sensitivity to the standard reference toxicant potassium dichromate, $K_2Cr_2O_7$ (from more sensitive to less sensitive species):

P. purpureum > H. akashiwo > A. ussuriensis > *C. muelleri*

However, this trend was not confirmed for the ZnS and CdS NPs tested in current study, suggesting different mode of action of metal sulfide particles. *C. muelleri* was the most sensitive species to metal-sulfide NPs both after 96 h and seven days of exposure (Table 3, Fig. 6). In case of $K_2Cr_2O_7$, microalgae cells were exposed to highly toxic Cr(VI) from dichromate ions, $Cr_2O_7^{2-}$ which are formed as a result of $K_2Cr_2O_7$ dissociation in water (Jun-Fei and Shi-Li, 2019). In contrast, CdS and ZnS nanocrystals are known to be slightly soluble in water (Chen et al., 2020). Apparently, the difference in microalgae species sensitivity to $K_2Cr_2O_7$ and metal sulfide NPs arises from different mechanisms of uptake and interactions of $Cr_2O_7^{2-}$ ions and NPs with biomolecules in the microalgae cell-wall (Gabbasova et al., 2017).

The high toxicity of metal-ion-containing NPs and the possibility of NPs to be taken up by microalgae cells with nutrition was shown in bioassays with common test-species such as *R. subcapitata* (Bouldin et al., 2008). Several reports demonstrated that individual NPs dispersed in water predominantly pass into the cell by non-phagocytic processes (Zhao et al., 2016; Malejko et al., 2019). It is known that the pore size of plant cell-wall is 5–20 nm (Ma and Yan, 2018). Thus, it can be assumed that the studied CdS and ZnS NPs with the average sizes of 7.0 nm and 4.2 nm, respectively, could penetrate microalgae cells

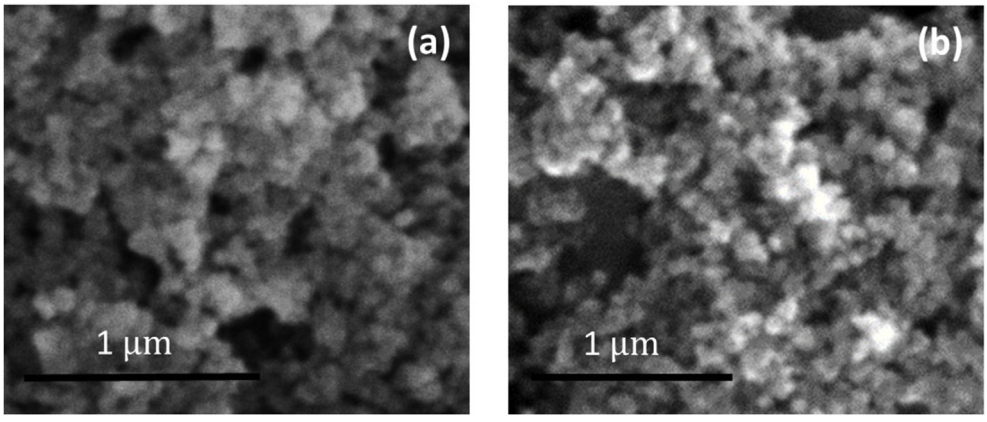

Fig. 2. SEM images of samples (a) CdS and (b) ZnS.

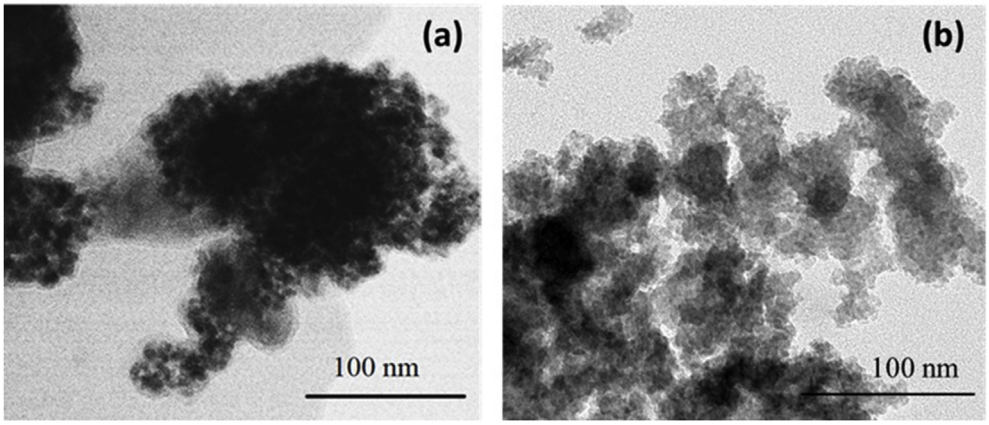

Fig. 3. TEM micrographs of samples (a) CdS and (b) ZnS.

through the pores of cell-walls and the general toxicity of both metal sulfides may be explained by this process.

However, we also observed some differences in the behavior of NPs towards the tested microalgae. In general, ZnS NPs were more toxic for *A. ussuriensis* and *H. akashiwo* species, while for *C. muelleri* and *P. purpureum* CdS NPs caused higher inhibition of growth rate (Table 3, Fig. 6). Probably, the sensitivity of different microalgae species to CdS and ZnS NPs depends on the chemical composition of NPs and their ability to interact with the components of microalgae cell-wall. Thus, the composition, size, and morphology of NPs are important for penetration into the algae cells and responsible for the toxicity levels of NPs.

It is known that microalgal cell-wall is composed of lipids, polysaccharides, and glycoproteins, and can form different chemical bonds with semiconductor NPs that depend on the nature of metal ion and donor atoms in biomolecules (Kumar et al., 2016; Neagu et al., 2017). It was previously reported that Zn^{2+} ions bind to oxygen- and nitrogen-containing ligands more easily, while Cd^{2+} ions prefer to coordinate to sulfur-containing ligands (Wu et al., 2018). The main light-harvesting pigment of the red microalgae *P. purpureum* is phycobilisome (Lee et al., 2019) which consists of nitrogen-rich molecules of phycobiliproteins (phycocyanin, phycoerythrin, and allophycocyanin) that can readily interact with ZnS NPs (Zhang et al., 2017).

We observed that the treatment of *P. purpureum* with ZnS caused a change in the algal cell pigmentation from red to olive green (Fig. 5c). This color change could occur as a result of the binding of zinc cations to phycoerythrin proteins (MacColl et al., 1994). A well-known fact is that red algae cells could change the number and composition of phycobilisomes to adapt light-harvesting complex to changes in light wavelength (Chenu et al., 2017) or as a compensation to a lack of nitrogen in the medium (Ruan et al., 2018).

Pigmental modification of *P. purpureum* is an important mechanism of algal adaptation to a high concentration of zinc that prevents the uptake of NPs and defends microalgae cells from their further toxic influence. For this reason, the red algae *P. purpureum* had the highest tolerance to ZnS, and microalgae cells did not reveal any changes of growth-rate after a 96-h exposure to ZnS even at the highest used concentration (100 mg/l) (Fig. 6a). This implies that they demonstrated the lowest sensitivity to ZnS NPs in comparison to the other species exposed for seven days (Fig. 6b). The higher ability of *P. purpureum* to absorb metal ions and tolerance of the red microalgae to Zn^{2+}, when compared with the other microalgae species, have been already demonstrated (Schmitt et al., 2001).

Additionally, we found that the cells of *P. purpureum* showed a significant enlargement after exposure to CdS NPs at high concentrations (Figs. 4d and 5b). This effect could be explained by the disorder of regulation between photosynthesis and carbon sequestration processes (Launay et al., 2019). Thus, algae cells retain their ability to fix carbon and accumulate organic matter, produced by photosynthesis, but lose their capability for cell division. Such a disorder could be induced by generation of reactive oxygen species (ROS) in the presence of CdS rather than ZnS (Yu et al., 2018; Pikula et al., 2019c).

CdS nanocrystals have a direct and relatively narrow band gap of 2.4 eV (Wu et al., 2017) which provides remarkable ROS production under visible light irradiation, especially at wavelengths shorter than 516 nm (Cheng et al., 2018). While, ZnS is known as a direct wide-gap photocatalyst with a band gap of 3.54 eV for cubic structured particles (Kim et al., 2020) which absorbs ultraviolet light with wavelength below 350 nm (Lee and Wu, 2017). Moreover, ZnS is known for its lower photocatalytic efficiency due to high charge-recombination rates and lower resistance to photocorrosion (Chen et al., 2020).

Considering the experimental conditions during the illumination of bioassay with a cool white fluorescent light (Table 1), the ROS production and potential aquatic toxicity related to the oxidative damage and disorders caused by free-radicals are expected to be higher for CdS NPs when compared with their ZnS counterparts. Moreover, the stability of CdS nanocrystals in water (log K_{s0}, –31.42) is higher than that of ZnS (log K_{s0}, –26.02) because the solubility product of CdS is lower (e.g. less Cd^{2+} and S^{2-} ions are formed in solution) (Chen et al., 2020). This means that CdS NPs would remain for a longer time as CdS nanocrystals in the surrounding media or inside the cell (if the NPs pass the cell membrane). Therefore, they will keep their ability to produce ROS, the latter species causing oxidative changes in the cell-wall substances or the intracellular substrates. Thus, the light-induced activity of CdS can contribute to the predominant oxidative mechanism of the CdS toxicity for *C. muelleri* and *P. purpureum* species.

4.2. Esterase activity inhibition

For both types of NPs after 3 h of exposure to microalgae, a high esterase activity inhibition was noticed (Table 3), which was probably caused by the stimulation of ROS production in microalgae cells under the influence of both CdS and ZnS nanocrystals (Pikula et al., 2019c). Further partial dissociation of the NPs leads to reduced ROS production rates and, subsequently, to lower esterase activity inhibition, as given in Table 3 for all microalgae species after their treatment for 24 h. As expected, the effect of more photoactive CdS NPs on the esterase activity inhibition was higher for all microalgae species compared with that of less photoactive ZnS. It is worth noticing a pronounced increase of calculated EC_{50} concentrations in the esterase activity inhibition for *A. ussuriensis* and *H. akashiwo* after 24 h of exposure to ZnS NPs (Table 3). Probably, the influence of ZnS NPs on enzyme activity of microalgae was lower because of the slow dissociation of ZnS nanocrystals to Zn^{2+} and S^{2-} ions with time and reduced production of ROS.

Table 3
Calculated values of EC_{50} for viability, esterase activity, and membrane potential of microalgae after exposure to nanomaterials, mg/l.

Species	Growth-rate inhibition/Viability			Esterase activity		Membrane potential	
	24 h	96 h	7 days	3 h	24 h	6 h	24 h
CdS							
A. ussuriensis	n/a	189.2 (197.4–198.9)	61.8 (61.4–62.2)	65.3 (64.8–65.7)	145.5 (144.2–146.8)	151.3 (142.8–160.5)	116.7 (116–117.3)
H. akashiwo	228.3 (223.0–233.9)	180.8 (180.1–181.4)	38.8 (38.4–39.1)	27.0 (26.5–27.6)	195.3 (193.8–196.8)	106.4 (100.7–112.5)	101.0 (99.5–102.2)
C. muelleri	n/a	10.4 (10.2–10.5)	3.0 (2.9–3.1)	235	n/a	264.7 (264.0–265.4)	61.1 (58.5–63.8)
P. purpureum	225.8 (224.7–226.9)	50.3 (48.7–51.9)	41.5 (40.5–42.5)	n/a	63.6 (63.1–64.1)	32.6 (32.3–32.9)	51.3 (50.8–51.8)
ZnS							
A. ussuriensis	206.0 (196.6–216.2)	108.2 (107.0–109.3)	42.9 (42.6–43.3)	77.9 (75.9–80.0)	410.0	n/a	n/a
H. akashiwo	132.9 (130.6–135.3)	119.3 (117.5–121.3)	27.9 (27.6–28.2)	97.2 (94.7–99.8)	375.1 (373.6–376.7)	163.7 (162.4–165.0)	224.8 (221.4–228.3)
C. muelleri	131.7 (131.1–132.3)	21.4 (20.9–21.9)	4.2 (4.1–4.2)	n/a	n/a	51.9 (51.1–52.6)	367.0
P. purpureum	n/a	n/a	197.5 (191.3–204.1)	n/a	n/a	n/a	hyperpolarization (19–21%) *

95% confidence limits presented in the parentheses.
n/a – measured effect was not observed even at the highest concentrations of the sample.
*Exposure to NPs caused a rise of measuring endpoint. The data were presented as the percentage increase of $DiOC_6$ fluorescence at the highest nanoparticle concentration (100 mg/l) compared to the control group.

4.3. Membrane potential changes

Dysfunction, deformation, and violation of cell-wall integrity are very dangerous for the health (or even the life) of the organisms. In animal cells, the intact cell membrane is a vital factor, because the membranes serve as the barriers as well as impart mechanical, and matrix properties to the organisms. Any defects may lead to changes in the elasticity of membranes, the disappearance of lipid microdomains, changes in permeability for cations, as well as variations of other characteristics (Engin et al., 2017; Seong and Lee, 2017). Such changes are known to lead to various diseases or make the cell easily susceptible to the attack of pathogens.

The results observed in the present study demonstrate different dynamics in microalgae membrane potential changes between 6 and 24 h of exposure to CdS and ZnS NPs (Table 3). For CdS, we can point out progressive depolarization of cell membranes with time expressed in a decrease of the calculated EC_{50} concentrations of membrane polarization for all the microalgae species except *P. purpureum*. In contrast, the EC_{50} concentration calculated for ZnS NPs increased with time, indicating a decrease of the NP effect on the microalgae membrane potential.

The observed microalgae cell membrane depolarization correlates with the photocatalytic properties of the tested NPs. The more stable CdS NPs are believed to provide a constant level of ROS production during the bioassay, thus provoking oxidative stress and membrane polarization disorder in microalgae cells. The lower effect of the ZnS NPs on cell membrane potential might be linked with photocorrosion of their nanocrystals, which would lead to reduced ROS production over time. Moreover, the microalgae cultivation during the treatment with NPs was provided by a visible light irradiation, which should stimulate the CdS NPs more efficiently than their ZnS counterparts (Lee and Wu, 2017; Cheng et al., 2018).

5. Conclusions

Summarizing the findings of the present research, we conclude that the sensitivity of different microalgae species to CdS and ZnS nanoparticles depends on particle size, chemical composition and their ability to interact with the components of the microalgal cell-wall. The general toxicity of the tested CdS and ZnS nanoparticles may also be related to their small size (7.0 and 4.2 nm, respectively), which allows them to pass an algal cell-wall through the pores. The ZnS nanoparticles were more toxic for *A. ussuriensis* and *H. akashiwo* species, while the CdS particles caused strong growth-rate inhibition for *C. muelleri* and *P. purpureum*. The red microalga *P. purpureum* demonstrated high tolerance to the ZnS nanoparticles, which could be explained by interaction of Zn ions with the phycobiliproteins in the red algae. The resistance of *P. purpureum* cells to the ZnS nanoparticles exposure is an interesting case for more detailed research in the future.

Based on the observations, we proposed different mechanisms of toxic action for the studied CdS and ZnS nanoparticles. Therefore, the higher influence of the CdS nanocrystals on morphological and biochemical changes of microalgal cells was based on the higher photoactivity of the CdS nanoparticles under visible-light irradiation and their higher stability in water. These properties allow CdS nanoparticles to generate more ROS, thus causing a higher risk of oxidative stress to aquatic organisms.

For a better understanding of aquatic toxicity of metal sulfide nanoparticles, several additional parameters must be considered in future research, such as the intensity of light and ultraviolet/visible irradiation, processes involved into ROS formation and further oxidation, as well as the transformation of NPs, and their transfer between different trophic levels of the food chain.

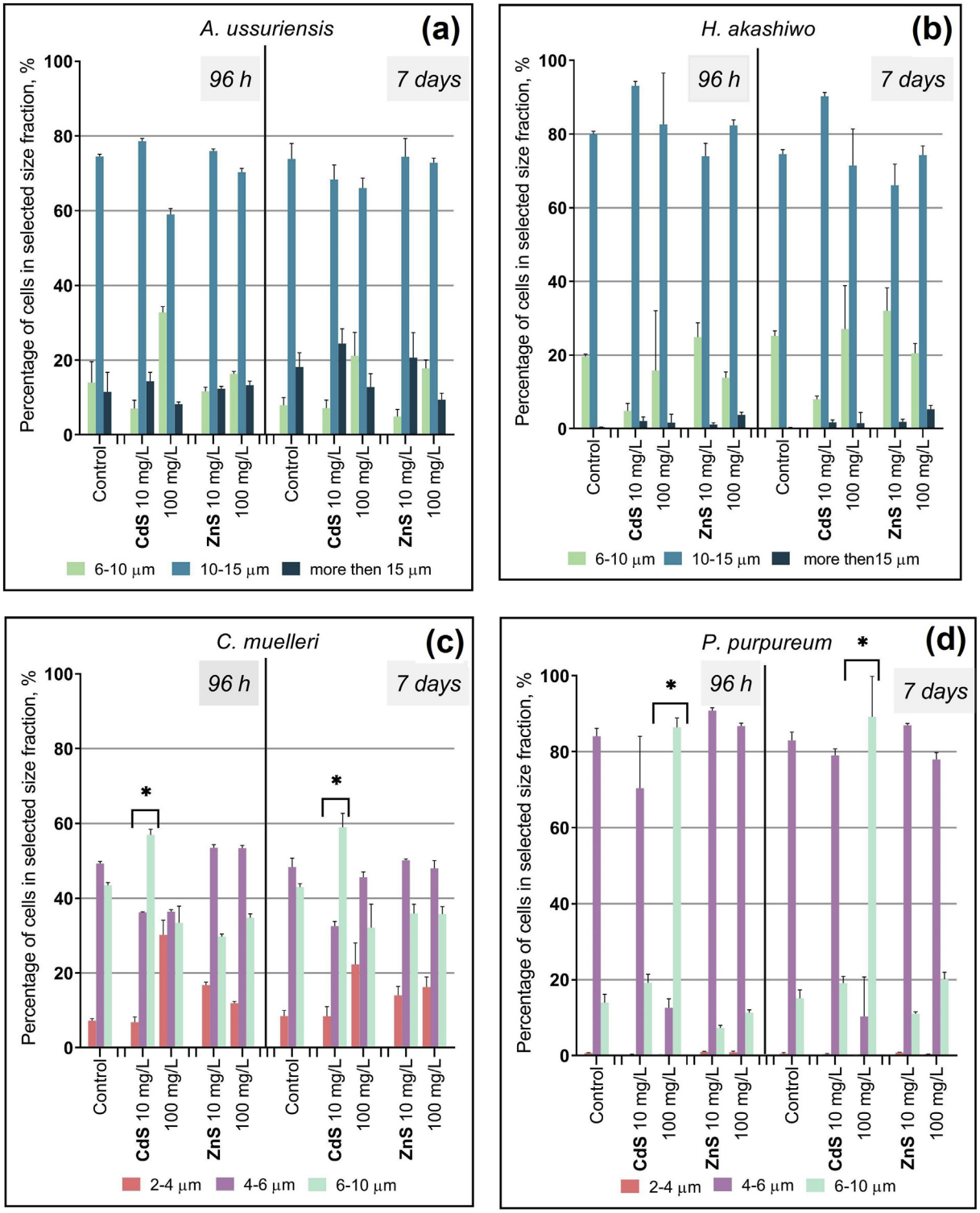

Fig. 4. Changes in microalgae cell size after 96 h and seven days of exposure to CdS and ZnS nanoparticles. (a) A. ussuriensis, (b) H. akashiwo, (c) *C. muelleri*, and (d) P. purpureum. *Significant change in microalgae cell size.

CRediT authorship contribution statement

Konstantin Pikula: Conceptualization, Methodology, Formal analysis, Investigation, Writing - original draft. **Neli Mintcheva:** Resources, Writing - review & editing. **Sergei A. Kulinich:** Resources, Writing - review & editing. **Alexander Zakharenko:** Conceptualization, Methodology, Visualization. **Zhanna Markina:** Resources, Validation. **Vladimir Chaika:** Resources, Methodology. **Tatiana Orlova:** Resources, Validation. **Yaroslav Mezhuev:** Validation, Writing - review & editing. **Emmanouil Kokkinakis:** Validation, Writing - review & editing. **Aristidis Tsatsakis:** Validation, Supervision. **Kirill Golokhvast:** Project administration, Funding acquisition.

Declaration of competing interest

The authors declare that they have no known competing financial

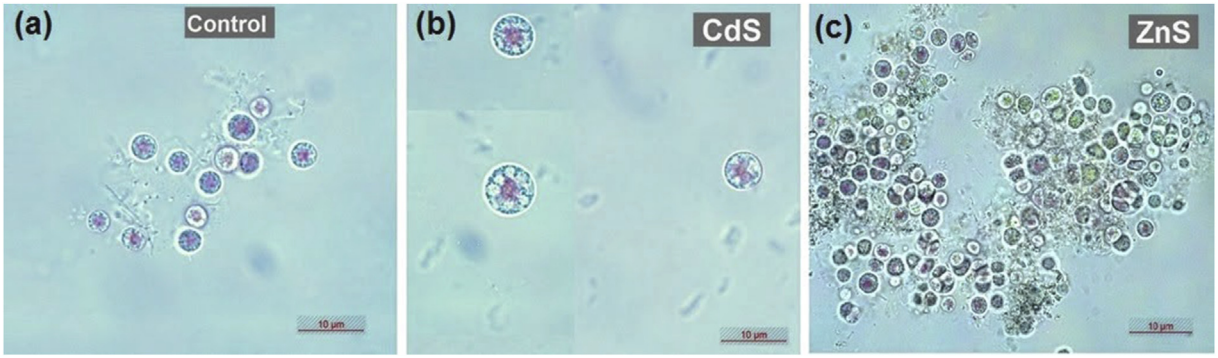

Fig. 5. P. purpureum after 96 h of exposure to CdS and ZnS nanoparticles. (a) Control group, (b) the cells exposed to CdS, and (c) the cells exposed to ZnS.

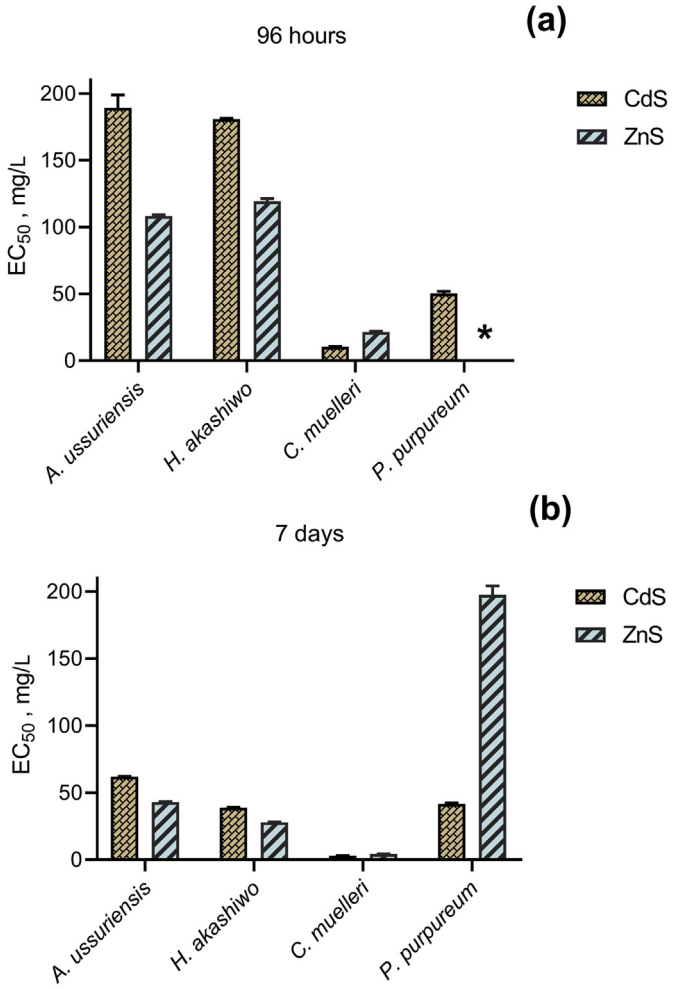

Fig. 6. Calculated EC_{50} concentrations of microalgae growth-rate inhibition after 96 h and seven days of exposure to CdS and ZnS nanoparticles. (a) 96-h exposure, (b) seven-days exposure. *Growth rate of microalgae has no changes even at the highest nanoparticle concentration (100 mg/l) compared to control group.

interests or personal relationships that could have appeared to influence the work reported in this paper.

Acknowledgements

This work was supported by the Russian Foundation for Basic Research (project number 19-05-50010). The authors are grateful to the FEFU Collective Use Center for providing scientific equipment. Dr. Muhammad Amjad Nawaz (Education and Scientific Center of Nanotechnology, Far Eastern Federal University, Vladivostok, Russian Federation) copy-edited this manuscript.

References

Balmuri, S.R., Selvaraj, U., Kumar, V.V., Anthony, S.P., Tsatsakis, A.M., Golokhvast, K.S., Raman, T., 2017. Effect of surfactant in mitigating cadmium oxide nanoparticle toxicity: implications for mitigating cadmium toxicity in environment. Environ. Res. 152, 141–149.

Bedia, J., Muelas-Ramos, V., Peñas-Garzón, M., Gómez-Avilés, A., Rodríguez, J.J., Belver, C., 2019. A review on the synthesis and characterization of metal organic frameworks for photocatalytic water purification. Catalysts 9 (1), 52.

Belver, C., Bedia, J., Gómez-Avilés, A., Peñas-Garzón, M., Rodriguez, J.J., 2019. Semiconductor photocatalysis for water purification. In: Nanoscale Materials in Water Purification. Elsevier, Amsterdam, pp. 581–651.

Bouldin, J.L., Ingle, T.M., Sengupta, A., Alexander, R., Hannigan, R.E., Buchanan, R.A., 2008. Aqueous toxicity and food chain transfer of quantum dots (TM) in freshwater algae and Ceriodaphnia dubia. Environ. Toxicol. Chem. 27 (9), 1958–1963.

Chen, S., Huang, D., Xu, P., Xue, W., Lei, L., Cheng, M., Wang, R., Liu, X., Deng, R., 2020. Semiconductor-based photocatalysts for photocatalytic and photoelectrochemical water splitting: will we stop with photocorrosion? J. Mater. Chem. 8 (5), 2286–2322.

Cheng, L., Xiang, Q., Liao, Y., Zhang, H., 2018. CdS-based photocatalysts. Energy Environ. Sci. 11 (6), 1362–1391.

Chenu, A., Keren, N., Paltiel, Y., Nevo, R., Reich, Z., Cao, J., 2017. Light adaptation in phycobilisome antennas: influence on the rod length and structural arrangement. J. Phys. Chem. B 121 (39), 9196–9202.

Crowley, L.C., Scott, A.P., Marfell, B.J., Boughaba, J.A., Chojnowski, G., Waterhouse, N.J., 2016. Measuring cell death by propidium iodide uptake and flow cytometry. Cold Spring Harb. Protoc. 2016 (7), pdb–prot087163.

Deng, Y., Xiao, Y., Zhou, Y., Zeng, T., Xing, M., Zhang, J., 2019. A structural engineering-inspired CdS based composite for photocatalytic remediation of organic pollutant and hexavalent chromium. Catal. Today 335, 101–109.

Drew, K., Ross, R., 1965. Some Generic Names in the Bangiophycidae. pp. 93–99 Taxon.

Engin, A.B., Nikitovic, D., Neagu, M., Henrich-Noack, P., Docea, A.O., Shtilman, M.I., Golokhvast, K.S., Tsatsakis, A.M., 2017. Mechanistic understanding of nanoparticles' interactions with extracellular matrix: the cell and immune system. Part. Fibre Toxicol 14 (1), 22.

Fontvieille, D.A., Outaguerouine, A., Thevenot, D.R., 1992. Fluorescein diacetate hydrolysis as a measure of microbial activity in aquatic systems- Application to activated sludges. Environ. Technol. 13 (6), 531–540.

Gabbasova, D.T., Matorin, D.N., Konyukhov, I.V., Seifullina, N.K., Zayadan, B.K., 2017. Effect of chromate ions on marine microalgae Phaeodactylum tricornutum. Microbiology 86 (1), 64–72.

Gao, J., Wang, Y., Folta, K.M., Krishna, V., Bai, W., Indeglia, P., Georgieva, A., Nakamura, H., Koopman, B., Moudgil, B., 2011. Polyhydroxy fullerenes (fullerols or fullerenols): beneficial effects on growth and lifespan in diverse biological models. PloS One 6 (5), e19976.

Grégori, G., Denis, M., Lefèvre, D., Beker, B., 2003. A flow cytometric approach to assess phytoplankton respiration. Advanced Flow Cytometry: Applications in Biological Research. Springer, Netherlands, Dordrecht, pp. 99–106.

Hara, Y., Chihara, M., 1987. Morphology, ultrastructure and taxonomy of the raphidophecean alga heterisigma-akashiwo. Bot. Mag. Tokyo 100 (2), 151–163.

Jun-Fei, Z., Shi-Li, L., 2019. Sensors for detection of Cr (VI) in water: a review. Int. J. Environ. Anal. Chem. https://doi.org/10.1080/03067319.2019.1675652.

Khataee, A., Movafeghi, A., Nazari, F., Vafaei, F., Dadpour, M.R., Hanifehpour, Y., Joo, S.W., 2014. The toxic effects of L-Cysteine-capped cadmium sulfide nanoparticles on the aquatic plant Spirodela polyrrhiza. J. Nanoparticle Res. 16 (12), 2774.

Kim, J., Lee, C.R., Arepalli, V.K., Kim, S.J., Lee, W.J., Chung, Y.D., 2020. Role of hydrazine in the enhanced growth of zinc sulfide thin films using chemical bath deposition for Cu (In, Ga) Se_2 solar cell application. Mater. Sci. Semicond. Process. 105, 104729.

Kim, J., Park, Y., Yoon, T.H., Yoon, C.S., Choi, K., 2010. Phototoxicity of CdSe/ZnSe quantum dots with surface coatings of 3-mercaptopropionic acid or tri-n-

octylphosphine oxide/gum Arabic in Daphnia magna under environmentally relevant UV-B light. Aquat. Toxicol. 97 (2), 116–124.
Kumar, D., Pandey, L.K., Gaur, J.P., 2016. Metal sorption by algal biomass: from batch to continuous system. Algal Res 18, 95–109.
Kumari, K., Singh, P., Bauddh, K., Mallick, S., Chandra, R., 2019. Implications of metal nanoparticles on aquatic fauna: a review. Nanosci. Nanotechnol. - Asia 9 (1), 30–43.
Labiadh, H., Sellami, B., Khazri, A., Saidani, W., Khemais, S., 2017. Optical properties and toxicity of undoped and Mn-doped ZnS semiconductor nanoparticles synthesized through the aqueous route. Opt. Mater. 64, 179–186.
Launay, H., Receveur-Bréchot, V., Carrière, F., Gontero, B., 2019. Orchestration of algal metabolism by protein disorder. Arch. Biochem. Biophys. 672, 108070.
Lee, G.-J., Wu, J.J., 2017. Recent developments in ZnS photocatalysts from synthesis to photocatalytic applications – a review. Powder Technol. 318, 8–22.
Lee, J., Kim, D., Bhattacharya, D., Yoon, H.S., 2019. Expansion of phycobilisome linker gene families in mesophilic red algae. Nat. Commun. 10 (1), 1–10.
Ma, X., Yan, J., 2018. Plant uptake and accumulation of engineered metallic nanoparticles from lab to field conditions. Curr Opin Environ Sci Health 6, 16–20.
MacColl, R., Williams, O., Eisele, L.E., Berns, D.S., 1994. Spectroscopic changes for c-phycocyanin and phycoerythrin-545 produced by ferric ion. Biochim. Biophys. Acta Bioenerg. 1188 (3), 398–404.
Malejko, J., Szymańska, N., Bajguz, A., Godlewska-Żyłkiewicz, B., 2019. Studies on the uptake and transformation of gold (III) and gold nanoparticles in a water–green algae environment using mass spectrometry techniques. J. Anal. At. Spectrom. 34 (7), 1485–1496.
Mansour, S., Knani, S., Bensouilah, R., Ksibi, Z., 2020. Wastewater problems and treatments. Current Trends and Future Developments on (Bio-) Membranes. Elsevier, Amsterdam, pp. 151–174.
Matos, B., Martins, M., Samamed, A.C., Sousa, D., Ferreira, I., Diniz, M.S., 2020. Toxicity evaluation of quantum dots (ZnS and CdS) singly and combined in zebrafish (Danio rerio). Int. J. Environ. Res. Publ. Health 17 (1), 232.
Mintcheva, N., Gicheva, G., Panayotova, M., Wunderlich, W., Kuchmizhak, A.A., Kulinich, S.A., 2019. Preparation and photocatalytic properties of CdS and ZnS nanomaterials derived from metal xanthate. Materials 12 (20), 3313.
Neagu, M., Piperigkou, Z., Karamanou, K., Engin, A.B., Docea, A.O., Constantin, C., Negrei, C., Nikitovic, D., Tsatsakis, A., 2017. Protein bio-corona: critical issue in immune nanotoxicology. Arch. Toxicol. 91 (3), 1031–1048.
Nikitin, O.V., Kuzmin, N.B., Nasyrova, E.I., Gliakina, M.V., Stepanova, N.Y., 2019. The effects of barley straw extract on the microalgae growth. IOP Conf. Ser. Earth Environ. Sci. 315 (4), 042051.
OECD, 2011. Test No. 201: Freshwater Alga and Cyanobacteria, Growth Inhibition Test. OECD Guidelines for the Testing of Chemicals. OECD Publishing, Paris.
Perez-Garcia, O., Escalante, F.M., de-Bashan, L.E., Bashan, Y., 2011. Heterotrophic cultures of microalgae: metabolism and potential products. Water Res. 45 (1), 11–36.
Perry, S.W., Norman, J.P., Barbieri, J., Brown, E.B., Gelbard, H.A., 2011. Mitochondrial membrane potential probes and the proton gradient: a practical usage guide. Biotechniques 50 (2), 98–115.
Pikula, K., Chaika, V., Zakharenko, A., Markina, Z., Vedyagin, A., Kuznetsov, V., Gusev, A., Park, S., Golokhvast, K., 2020b. Comparison of the level and mechanisms of toxicity of carbon nanotubes, carbon nanofibers, and silicon nanotubes in bioassay with four marine microalgae. Nanomaterials 10 (3), 485.
Pikula, K.S., Chernyshev, V.V., Zakharenko, A.M., Chaika, V.V., Waissi, G., Hien, T.T., Hai, T.T., Tsatsakis, A.M., Golokhvast, K.S., 2019a. Toxicity assessment of particulate matter emitted from different types of vehicles on marine microalgae. Environ. Res. 179, 108785.
Pikula, K.S., Zakharenko, A.M., Aruoja, V., Golokhvast, K.S., Tsatsakis, A.M., 2019c. Oxidative stress and its biomarkers in microalgal ecotoxicology. Curr. Opin. Toxicol. 13, 8–15.
Pikula, K.S., Zakharenko, A.M., Chaika, V.V., Kirichenko, K.Y., Tsatsakis, A.M., Golokhvast, K.S., 2020a. Risk assessment in nanotoxicology: bioinformatics and computational approaches. Curr. Opin. Toxicol. 19, 1–6.
Pikula, K.S., Zakharenko, A.M., Chaika, V.V., Stratidakis, A.K., Kokkinakis, M., Waissi, G., Rakitskii, V.N., Sarigiannis, D.A., Hayes, A.W., Coleman, M.D., Tsatsakis, A., Golokhvast, K.S., 2019b. Toxicity bioassay of waste cooking oil-based biodiesel on marine microalgae. Toxicol. Rep. 6, 111–117.
Piperigkou, Z., Karamanou, K., Engin, A.B., Gialeli, C., Docea, A.O., Vynios, D.H., Pavãoc, M.S.G., Golokhvast, K.S., Shtilman, M.I., Argiris, A., Shishatskaya, E., Tsatsakis, A.M., 2016. Emerging aspects of nanotoxicology in health and disease: from agriculture and food sector to cancer therapeutics. Food Chem. Toxicol. 91, 42–57.
Prado, R., Rioboo, C., Herrero, C., Cid, Á., 2012. Screening acute cytotoxicity biomarkers using a microalga as test organism. Ecotoxicol. Environ. Saf. 86, 219–226.
Ruan, Z., Prášil, O., Giordano, M., 2018. The phycobilisomes of Synechococcus sp. are constructed to minimize nitrogen use in nitrogen-limited cells and to maximize energy capture in energy-limited cells. Environ. Exp. Bot. 150, 152–160.
Sabnis, R.W., Deligeorgiev, T.G., Jachak, M.N., Dalvi, T.S., 1997. DiOC(6)(3): a useful dye for staining the endoplasmic reticulum. Biotech. Histochem. 72 (5), 253–258.
Schmitt, D., Müller, A., Csögör, Z., Frimmel, F.H., Posten, C., 2001. The adsorption kinetics of metal ions onto different microalgae and siliceous earth. Water Res. 35 (3), 779–785.
Seong, M., Lee, D.G., 2017. Silver nanoparticles against Salmonella enterica serotype typhimurium: role of inner membrane dysfunction. Curr. Microbiol. 74 (6), 661–670.
Silva, B.F., Andreani, T., Gavina, A., Vieira, M.N., Pereira, C.M., Rocha-Santos, T., Pereira, R., 2016. Toxicological impact of cadmium-based quantum dots towards aquatic biota: effect of natural sunlight exposure. Aquat. Toxicol. 176, 197–207.
Singh, P., Borthakur, A., Mishra, P.K., Tiwary, D. (Eds.), 2020. Nano-materials as Photocatalysts for Degradation of Environmental Pollutants: Challenges and Possibilities. Elsevier, Amsterdam, pp. 65–127.
Suzuki, T., Fujikura, K., Higashiyama, T., Takata, K., 1997. DNA staining for fluorescence and laser confocal microscopy. J. Histochem. Cytochem. 45 (1), 49–53.
Wang, R., Hua, M., Yu, Y., Zhang, M., Xian, Q.M., Yin, D.Q., 2016. Evaluating the effects of allelochemical ferulic acid on Microcystis aeruginosa by pulse-amplitude-modulated (PAM) fluorometry and flow cytometry. Chemosphere 147, 264–271.
Wu, A., Tian, C., Jiao, Y., Yan, Q., Yang, G., Fu, H., 2017. Sequential two-step hydrothermal growth of MoS_2/CdS core-shell heterojunctions for efficient visible light-driven photocatalytic H_2 evolution. Appl. Catal., B 203, 955–963.
Wu, H., Zhang, X., Yin, X., Inaba, Y., Miki, H., Takeshita, K., 2018. Selective separation of cadmium (II) from zinc (II) by a novel hydrophobic ionic liquid including an N, N, N′, N′-tetrakis (2-methylpyridyl)-1, 2-phenylenediamine-4-amido structure: a hard–soft donor combined method. Dalton Trans. 47 (30), 10063–10070.
Xu, C., Anusuyadevi, P.R., Aymonier, C., Luque, R., Marre, S., 2019. Nanostructured materials for photocatalysis. Chem. Soc. Rev. 48 (14), 3868–3902.
Yu, Z., Hao, R., Zhang, L., Zhu, Y., 2018. Effects of TiO_2, SiO_2, Ag and CdTe/CdS quantum dots nanoparticles on toxicity of cadmium towards Chlamydomonas reinhardtii. Ecotoxicol. Environ. Saf. 156, 75–86.
Zhang, H., Meng, D., Fu, B., Fan, H., Cai, R., Fu, P.P., Wu, X., 2019. Separation of charge carriers and generation of reactive oxygen species by TiO_2 nanoparticles mixed with differently-coated gold nanorods under light irradiation. J. Environ. Sci. Health Part C Environ. Carcinog. Ecotoxicol. Rev. 37 (2), 81–98.
Zhang, J., Ma, J., Liu, D., Qin, S., Sun, S., Zhao, J., Sui, S.F., 2017. Structure of phycobilisome from the red alga Griffithsia pacifica. Nature 551 (7678), 57–63.
Zhao, J., Cao, X., Liu, X., Wang, Z., Zhang, C., White, J.C., Xing, B., 2016. Interactions of CuO nanoparticles with the algae Chlorella pyrenoidosa: adhesion, uptake, and toxicity. Nanotoxicology 10 (9), 1297–1305.
Zhao, Q., Chen, A.N., Hu, S.X., Liu, Q., Chen, M., Liu, L., Shao, C.L., Tang, X.X., Wang, C.Y., 2018. Microalgal microscale model for microalgal growth inhibition evaluation of marine natural products. Sci. Rep. 8 (1), 1–10.